Dual-band slot-loaded patch antenna

S. Maci
G. Biffi Gentili
P. Piazzesi
C. Salvador

Indexing terms: Multifrequency antennas, Method of moments, Stacked antenna, Slot-loaded antenna

Abstract: A new patch antenna is analysed which provides dual-frequency operation by means of two narrow slots close to the patch radiating edges. The two modes of operations show similar radiating properties. The ratio between the two frequencies can be well controlled within a range varying from 1.6 to 2, by using simple semi-empirical formulas derived from a physical model and tested by using a fullwave analysis. To obtain a more extended range of this frequency ratio, two tuning microstrip stubs are introduced on a back substrate. Satisfactory performances of simultaneous matching when using a single feed point is demonstrated. Several measurements are shown for both the input impedance and the radiation pattern.

1 Introduction

Radar and communication systems such as synthetic aperture radar (SAR) and global position system (GPS) often require dual or multifrequency operations; a unique radiating structure would be desirable to accomplish these operations. An ideal two-frequency antenna should have a similar performance in both operating modes in terms of radiating properties and simultaneous matching. It is not a straightforward matter to obtain these features using planar technologies. On the other hand, planar antennas show the well known advantages of low cost, low weight and conformability, and their use in double-frequency applications appears very attractive.

The multifrequency patch angennas found in the literature can be subdivided into two categories, namely; multiresonator antennas and reactive loading antennas. In the first kind of structure, multifrequency behaviour is obtained by means of multiple radiating elements, each supporting strong currents and radiation at resonance. This category includes multilayer stacked-patch antennas fabricated by using circular [1], annular [2], rectangular [3], and triangular [4] patches. A multiresonator printed antenna can also be fabricated on a single dielectric layer by using aperture-coupled parallel rectangular dipoles [5]. Unfortunately, the design of the frequency ratio (FR) parameter is not a straightforward matter for all the multiresonators structures since simple and accurate design formulas are not yet available in the literature.

The reactive-loading patch antenna consists of a single radiating element in which the double resonant behaviour is obtained by connecting coaxial [6] or microstrip [7] stubs at the radiating edge of a rectangular patch. This solution cannot allow an FR higher than 1.2. Higher values of FR (4–5) can be obtained by using two lumped capacitors connected from the patch to the ground plane [8]. In References 9 and 10 the double-frequency behaviour is obtained by means of shorting vias symmetrically located with respect to the patch axes.

Another kind of reactive loading can be introduced by etching slots on a patch. The slot loading allows to strongly modify the resonant mode of a rectangular patch, particularly when the slots cut the current lines of the unperturbed mode. In particular, as shown in Reference 11, the simultaneous use of slots and short-circuit vias, allows to obtain an FR from 1.3 to 3 depending on the number of vias.

In this paper, a particular kind of slot-loaded patch antenna (SPA) is studied. Its structure has been independently introduced in References 12 and 13 and consists of a rectangular patch with two narrow slots etched close and parallel to the radiating edge. The new antenna offers a good compromise between structural complexity and electromagnetic features such as efficiency and cross-polar radiation.

In Section 2, the basic configuration is described and the physical behaviour is illustrated by referring to the current line distributions at the two resonances. The design parameters are exhaustively investigated in Section 3, where simple empirical formulas for predicting the resonant frequencies are given in which the physical behaviour of the SPA is easily readable. The accuracy of these formulas has been tested by means of a fullwave analysis. To this end, a method of moments (MoM) in a rectangular waveguide domain has been used according to the formulation in Reference 15, that involves roof-top basis functions. To make this closed-domain formulation suitable for planar antennas analysis the waveguide was filled by a high layer of slightly lossy medium, as suggested in References 12 and 14.

By using the design formulas the FR can be varied in a range varying from 1.6 to 2. Although this range can cover several cases of practical applications, lower values of FR are sometimes required. A simple arrangement that allows extension of the lower limit of the FR is proposed in Section 4.

Section 5 is focused on the problem of the simultaneous matching at both frequencies by using a single feed point that can be used to reduce the complexity and cost

Paper 1932H (E11), first received 12th October 1994 and in revised form 13th March 1995

The authors are with the Department of Electronic Engineering, University of Florence, Via S. Marta 3, 50135, Florence, Italy

of the radiating element, particularly in view of its use in arrays structures. Finally, in Section 6, measurements of the input reflection coefficient, the gain and radiation pattern are presented and discussed in comparison with numerical results.

2 Basic structure

The geometry of the slot-loaded patch antenna (SPA) is shown in Fig. 1. Two narrow slots with dimensions L_s

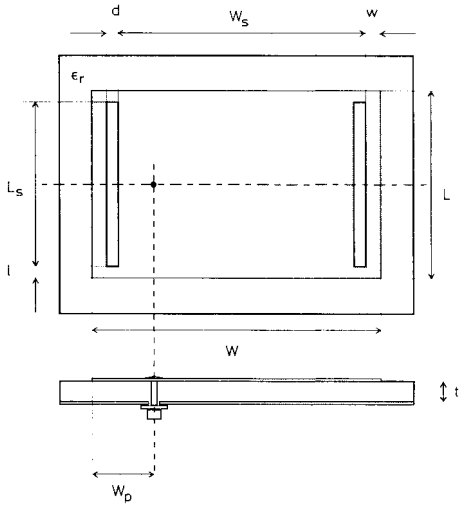

Fig. 1 *Geometry of probe feed SPA*

and d are etched on the rectangular patch close and parallel to the radiating edges of the patch. The location of the slots with respect to the patch is defined by the dimensions w and l. In the basic configuration, they are very small with respect to the dimensions L and W of the patch. The SPA can be fed by a probe or a coupling aperture. Here, the probe feed is used, but most of the consideration on the antenna properties apply as well to aperture coupling [13].

The resonant behaviour of the SPA may be explained by starting from the cavity model description of an unslotted rectangular patch. The first three modes that can be excited in the cavity are usually denoted by TM_{100}, TM_{200} and TM_{300}. These modes correspond to longitudinal currents distributed on the patch which have nulls at the radiating edges. The TM_{100} is the most used in practical applications since the TM_{200} mode has a broadside-null radiation pattern and the TM_{300} produces grating lobes.

When the two narrow slots are etched close to the radiating edges (small values of l and w), minor perturbations of TM_{100} are expected because the slots are located close to the current minima. In this case, the patch current distribution is like that sketched in Fig. 2*a*. The radiative mechanism associated with this first mode is essentially the same as that of a patch without slots. As a consequence, its resonant frequency is only slightly different from that of a standard patch.

On the other hand, the slots are located where the current of the unperturbed TM_{300} should be significant, so that this current is strongly modified and assumes the distribution depicted on Fig. 2*b*. The currents circulate around the slot and find a resonant condition with nulls close to the two edges of each slot. This condition forces the central portion of the current distribution to be broader than that associated with an unperturbed

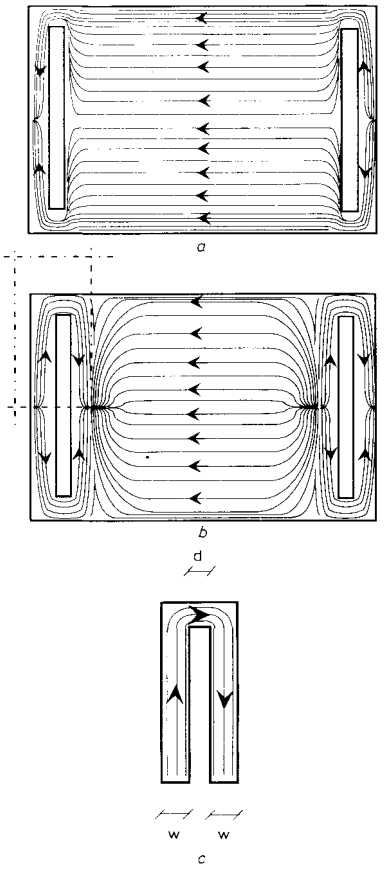

Fig. 2 *Current distributions on slotted patch*
$W = 40$ mm, $L = 30$ mm, $d = 1$ mm, $Ls = 28$ mm, $Ws = 36$ mm
(*a*) TM_{100} mode
(*b*) TM_{300} mode
(*c*) equivalent model (half-wavelength microstrip resonator)

TM_{300}, and becomes similar to that of the TM_{100} mode. The perturbed TM_{300} mode has two properties; the resonant frequency is considerably lowered and, as shown subsequently, the radiation pattern loses the typical three-lobe shape of the unperturbed TM_{300} mode and becomes similar to that of the TM_{100} mode.

The perturbation of the TM_{300} current distribution also depends on the slot length that can lead to a significant deformation in the radiation pattern. Fig. 3 shows the effect of a reduction of the slot length on the TM_{300} radiation pattern. The results have been obtained by the method of moments (MoM) analysis described in Reference 12. The E-plane far-field pattern is considered for a SPA with $w = d = t = L/30 = W/40$. The various plots refer to different values of l. The current distributions of the TM_{300} resonances are shown in the insets of the same Figure. For short slots (*a*), the radiation pattern has three lobes such as that of an unperturbed TM_{300} mode. When the slot length increases (*b*), the central lobe reduces and disappears when the far-field contribution of the current

circulating around the slots completely cancels out the contribution of the currents in the central portion. This last mentioned contribution becomes gradually stronger

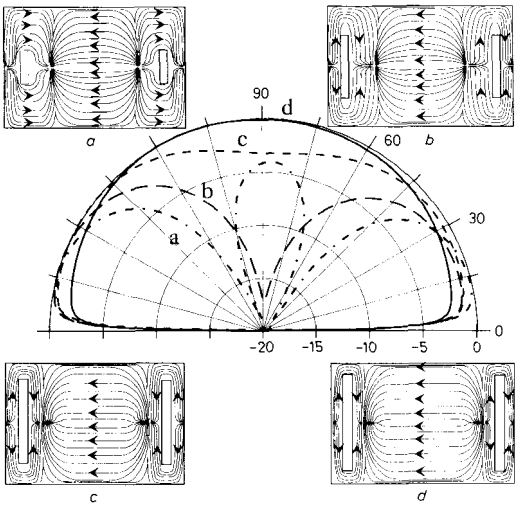

Fig. 3 *Current distributions and E-plane far field pattern of SPA for TM_{300} mode*
$w = d = t = L/30 = W/40$
(*a*) $l = L/30$
(*b*) $l = 4L/30$
(*c*) $l = 5L/30$
(*d*) $l = 7L/30$

when the slot length further increases, due to a larger extension of the central currents. The radiation pattern becomes increasingly similar to that of a standard patch in the TM_{100} configuration (*c*), (*d*). In the process described, the resonant frequency gradually decreases as can be inferred by the broadening of the central venter of the current distribution. Furthermore, the currents circulating around the slots give lower crosspolar distributions in the principal planes, as can be inferred from the antisymmetry of the current distribution.

3 Design criteria and parametric analysis

The best antenna performance in terms of both radiative properties and simultaneous impedance matching at the two operating frequencies is obtained when the width d of the two slots is comparable with the thickness t of the substrate and when

$$\frac{W}{50} < w < \frac{W}{15}; \quad l < \frac{L}{10} \tag{1}$$

Furthermore, to ensure a good radiation efficiency at both frequencies, the aspect ratio between the two sides of the patch is fixed in the range

$$0.7 < L/W < 0.8 \tag{2}$$

Denote by f_{100} and f_{300} the resonant frequencies associated with the modified TM_{100} and TM_{300} modes, respectively. To design the two frequencies, simple semi-empirical formulas based on physical models have been found very useful. As mentioned previously, the first resonance is not much affected by slot loading, so that its frequency can be predicted by slightly modifying the well established formula for rectangular, unslotted patches; i.e.

$$f_{100} = \frac{c}{2(W + \Delta W' + \Delta W'')\sqrt{[\varepsilon_e(L/t, \varepsilon_r)]}} \tag{3}$$

where c is the free-space speed of light,

$$\varepsilon_e(x, y) = \frac{y+1}{2} + \frac{y-1}{2}\left[1 + \frac{10}{x}\right]^{-1/2} \tag{4}$$

and

$$\Delta W' = W\left(1.5\,\frac{w}{W} - 0.4\,\frac{l}{L}\right) \tag{5a}$$

$$\Delta W'' = g\left(\frac{L}{t}, \varepsilon_T\right)t \tag{5b}$$

where

$$g(x, y) = \frac{1}{\pi}\frac{x + 0.336}{x + 0.556} \times \left[0.28 + \frac{y+1}{y}(0.274 + \ln(x + 2.518))\right] \tag{6}$$

It is worth noting that the equivalent overlength $\Delta W''$ is that suggested in Reference 16 for standard rectangular patches. The loading effect of the slot is effectively modelled by the term $\Delta W'$ that depends on l and w. Its expression has been derived by fitting the data provided by the MoM analysis in the range

$$0.7 < \frac{L}{W} < 0.8 \tag{7a}$$

$$\frac{w}{W} < \frac{1}{20}; \frac{l}{L} < \frac{1}{10}; \frac{t}{L} < \frac{1}{10}; \frac{d}{W} < \frac{1}{25} \tag{7b}$$

The upper resonant frequency was predicted according to a simple transmission line model, which is derived by a direct inspection of the current distribution at the modified TM_{300} mode (Fig. 2*b*). As described in the previous Section, the side currents find a resonant condition by circulating around the slots. The narrow portion of the conductor that encircles the slot behaves like two half-wavelength open-circuit stubs, as schematised in Fig. 2*c*. The effective dielectric constant of these equivalent stubs can be determined by assuming a w-width microstrip line model to describe the current distribution around the slot. This allows to predict the second resonant frequency according to

$$f_{300} = \frac{c}{2(L - 2l + d)\sqrt{[\varepsilon_e(w/t, \varepsilon_r)]}} \tag{8}$$

Although eqn. 8 is purely based on a physical model and does not include any empirical parameters based on data fitting, its accuracy has been successfully tested using the MoM analysis described in Reference 12 in the range given by eqns. 7. Table 1 shows the maximum relative differences between the resonant frequencies evaluated from eqns. 3 and 8 and from the MoM analysis. The results shown in the Table have been obtained by keeping constant the substrate ($t = 1.6$ mm, $\varepsilon_r = 2.2$), $L = 21$ mm and $L/W = 0.71$. For other values of t/L, the maximum deviation between the formulas and fullwave results was found to be lower than 3%. It is worth noting that the distance between the two slots does not appear in eqn. (8). In other words, the resonant condition of the TM_{300}

mode is assumed independent of the central portion of the current distribution that, on the other hand, plays an important role on the radiation effects. Although this

Table 1: Maximum relative differences between resonant frequencies evaluated from eqns. 3 and 8

Parameter range	$\varepsilon_{max}(f_{100})$	$\varepsilon_{max}(f_{300})$
	%	%
$\frac{l}{L}=\frac{1}{20}; \frac{d}{W}=\frac{1}{30}; \frac{w}{W}<\frac{1}{20}$	1.4	1.7
$\frac{w}{W}=\frac{1}{30}; \frac{d}{W}=\frac{1}{30}; \frac{l}{L}<\frac{1}{10}$	1.2	1.3
$\frac{l}{L}=\frac{1}{20}; \frac{w}{W}=\frac{1}{30}; \frac{d}{W}<\frac{1}{25}$	1.2	2.0

approximation could seem to be drastic, it is confirmed by the fullwave analysis, but only within the range expressed by eqns. 7.

For the sake of convenience, curves obtained from eqns. 3 and 8 are presented in Fig. 4. These curves are

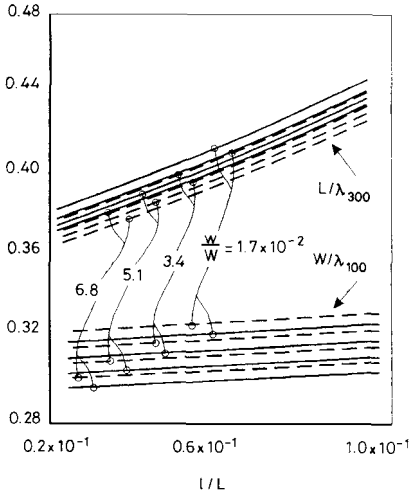

Fig. 4 *W/λ_{100} and L/λ_{300} against l/L for values of w/W*
$\lambda_{i00} = c/f_{i00}$; $i = 1, 3$; $\varepsilon_r = 2.2$; $d/L = 0.038$; $L/W = 0.71$
- - - - $t/L = 0.038$
—— $t/L = 0.076$

useful for understanding the behaviour of the antenna when changing the most important parameters; and may be directly used for a first step in the design effort. In particular, all the curves have been obtained by keeping constant the width of the slot ($d/L = 0.038$) and the dielectric constant ($\varepsilon_r = 2.2$). Furthermore, the two dimensions of the patch are fixed to $L = 21$ mm and $W = 29.5$ mm; anyhow, all the parameters are conveniently normalised in such a way to use the curves whenever $L/W = 0.71$. In particular, Fig. 4 shows the variation of the two parameters W/λ_{100} and L/λ_{300} against l/L for different values of w/W, where $\lambda_{i00} = c/f_{i00}$ ($i = 1, 3$). The results have been calculated for two values of the substrate thickness ($t/L = 0.038$, dashed line, and $t/L = 0.076$, continuous line). As mentioned, the curves associated with L/λ_{300} exhibit higher variation with respect to those of W/λ_{100}. This confirms the capability of adjusting only the third resonant frequency by changing l/L.

From Fig. 4 it can be inferred that the FR $r = f_{300}/f_{100}$ has different limitations depending on the thickness t. For example, for $t/L = 0.038$ $r \in (1.65, 1.85)$, for $t/L = 0.076$ $r \in (1.75, 1.95)$. These ranges are associated with $L/W = 0.71$; by increasing L/W, the range of r shifts to lower values. For example, when $W/L = 0.8$ a shift of 3% has been found for the extremes of the ranges indicated. Eventually one can design the frequency ratio within the range

$$1.6 < r < 2 \tag{9}$$

by properly choosing the aspect ratio and the slot length. To extend this range, the arrangement proposed in the following Section can be used.

4 Resonant tuning stubs

The ratio between the two frequencies which may be obtained with the SPA, is subjected to eqn. 9. Some applications, such as in GPS or radar systems, require a lower frequency ratio which is difficult to achieve with the simple configuration discussed. The range of FR may be extended by using the arrangement sketched in Fig. 5.

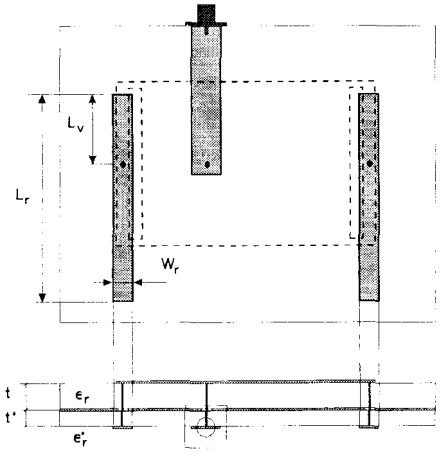

Fig. 5 *Geometry of SPA with tuning microstrip resonators*

In particular, two microstrip resonating stubs are printed on a back-substrate, and connected with the patch by two vias through the groundplane in a point between the slots and the radiating edge. The same arrangement may be used for the feeding structure. In particular, a via through the ground plane is connected with an open-ended microstrip feeding line.

In the via through of the resonant stubs, the unperturbed distribution of the electric current on the patch has a null for both resonant modes (Fig. 2), thus producing a strong reactive-loading effect. In particular, the two stubs are designed for resonating at a frequency falling between the two actual frequencies of the unloaded structure. They show either an inductive or a capacitive loading at TM_{100} or TM_{300}, respectively. This provides increase of f_{100} and decrease of f_{300}, thus allowing to obtain lower FR.

The two resonant stubs are essentially characterised by three parameters, namely the width w_r and the length L_r of the resonator, and the position L_v of the via. The first parameter, although less important in the design of the two frequencies, is dictated by the need to minimise the back radiation and the ohmic losses. As mentioned, the length L_r of the stubs has to be dimensioned in such a

way that the resonant frequency

$$f_r = \frac{c}{2(L_r + t'g(w_r/t'\varepsilon_r'))\sqrt{[\varepsilon_e(w_r/t', \varepsilon_r')]}} \quad (10)$$

falls between the two frequencies f_{100} and f_{300} of the SPA. In eqn. 10 $g(x, y)$ and ε_e are the same as those defined in eqns. 5 and 3. A good choice of the length resonators is $L_r = L_{r0}$, that is defined as the length associated with the resonant frequency

$$f_{r0} = \sqrt{(f_{100} f_{300})} \quad (11)$$

namely the geometric mean of the characteristic frequency of the unloaded SPA. The third parameter L_v greatly influences the ratio $r' = f'_{300}/f'_{100}$ between the two frequencies after introducing the resonators. By assuming L_r = const., the position L_v of the via does not affect the geometric mean value of the operating frequencies. On the other hand, the two frequencies gradually approach each other and the frequency ratio r' decreases. This is due to the different reactive loading at the two frequencies. Experimental data presented in Fig. 6, show the behaviour of r' and

$$\xi = \frac{\sqrt{(f'_{100} f'_{300})}}{f_{r0}} \quad (12)$$

as a function of both L_r (Fig. 6*a*) and L_v (Fig. 6*b*). These results have been obtained by a basic configuration of the SPA ($L = 31$ mm, $W = 42$ mm, $l = w = d = 1$ mm, $t = t' = 0.8$ mm, $\varepsilon_r = \varepsilon_r' = 2.2$) and by using microstrip resonant stubs with $W_r = 1$ mm. Further details on the experimental set are given in Section 6. Fig. 6*b* clearly shows that ξ is almost constant when changing L_v, and its value is close to unity. On the other hand, r' covers a range

$$1.1 < r' < 1.4 \quad (13)$$

when changing L_v/L_{ro} from 0.09 to 0.4. This range depends on the frequency ratio r of the SPA without stubs. In the case illustrated in Fig. 6, this ratio is 1.68.

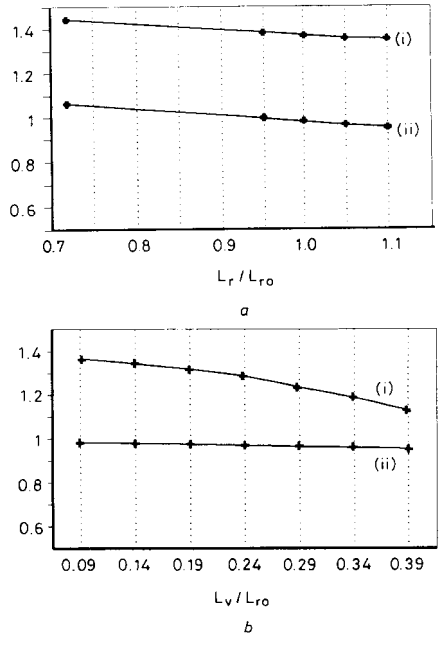

Fig. 6 *Experimental data for SPA*
$L = 31$ mm; $W = 42$ mm; $l = w = d = 1$ mm, $t = t' = 0.8$ mm; $\varepsilon_r = \varepsilon_r' = 2.2$; $f_{100} = 2.28$ GHz; $f_{300} = 3.57$ GHz
tuning microstrip resonators $W_r = 1$ mm
(i) $f_{ro} = \sqrt{(f_{100} f_{300})}$
(ii) $\xi = \sqrt{[(f'_{100} f'_{300})]}/f_{ro}$; $r' = f'_{300}/f'_{100}$
(*a*) L_r/L_{ro}
(*b*) L_v/L_{ro}

The two operating frequency of the stub-loaded SPA can be designed by using commercial CAD software for microwave networks. To this end, the SPA can be considered as a three-port network in which one port is connected with the input probe and the other ports with the, two vias. When the SPA scattering parameters are obtained by measurements or fullwave analysis, the design procedure reduces to a network synthesis of the two stubs. The stub loading of the SPA is also a dissipation source owing to radiation effects and ohmic losses. The radiation effects can be reduced by properly choosing the substrate properties and the stub width. It has been seen that the radiation may slightly affect the efficiency and the front-to-back ratio for FR close to unity.

5 Simultaneous impedance matching

One of the most promising aspects of the new antenna consists in the capability of matching the input impedance at two frequencies with a single feed point. As is well known, the location of the feeding point strongly affects the impedance level. For conventional patches, the impedance level increases as the feeding point moves towards an edge. It is always possible to find an optimum location for matching the impedance of the feeding line. Fig. 7 shows the amplitude of the input reflection coefficient at the two frequencies as a function of the probe position W_p. The data has been obtained by the fullwave analysis [12] applied to a patch with $W = 25$ mm, $L = 21$ mm, $L_s = 19$ mm, $w = 1$ mm, $d = 1$ mm, $t = 0.8$ mm, $\varepsilon_r = 2.2$. The via was connected by a 50Ω microstrip line. The curves associated with the two frequencies show minima for $W_p = 0.4W$ and $W_p = 0.42W$ for f_{100} and f_{300}, respectively. The optimum location of the feeding point has been found to be $W_p = 0.41W$ at the intersection of the two curves corresponding to a simultaneous impedance matching of −16 dB. The simultaneous matching is very sensitive to the feed-point position. For example, in the case described, a 1% error in the probe location causes a variation of 5 dB in the

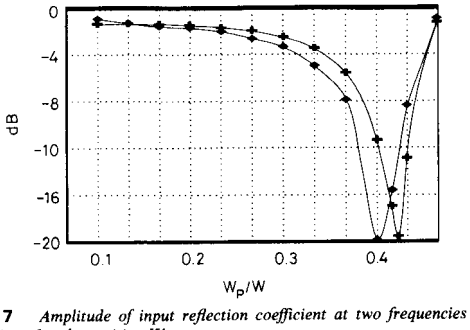

Fig. 7 *Amplitude of input reflection coefficient at two frequencies as function of probe position W_p*
$W = 25$ mm; $L = 21$ mm; $L_s = 19$ mm; $w = 1$ mm; $d = 1$ mm; $t = 0.8$ mm; $\varepsilon_r = 2.2$; 50Ω coaxial feed
+—+ $|S_{11}(f_{300})|$
◆—◆ $|S_{11}(f_{100})|$

input reflection coefficient level. In its practical realisation, the simultaneous tuning can be obtained by slightly shifting the input point in the direction that is suggested by the previous plots.

Another parametric analysis was carried out to investigate the effect of the slot length and position on the dual-matching capability. From this analysis we inferred that a good performance is obtained when l/L and w/W assume values within the range defined in eqn. 1.

6 Experimental results

Experiments were carried out to validate the numerical analysis of the input impedance and to verify the gain performance at both frequencies. Several prototypes at simultaneous C- and X-bands with and without resonant stubs were fabricated on RT Duroid 5880 ($\varepsilon_r = 2.2$, $t = 0.8$ mm, $\mathrm{tg}\delta = 5 \times 10^{-4}$) and tested by the HP 8510 network analyser. A time-domain gating was applied to remove the connector discontinuities of the probe feed. Fig. 8 shows the amplitude of the reflection coefficient for

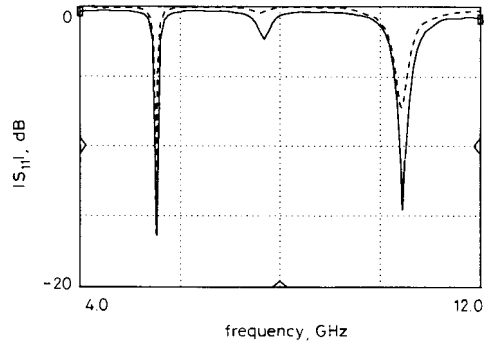

Fig. 8 *Amplitude of input reflection coefficient for SPA without tuning resonators fed by 50Ω coaxial probe*

$W = 15.5$ mm; $L = 11.5$ mm; $l = 0.5$ mm; $w = 1$ mm; $d = 1$ mm; $W_p = 5.5$ mm; $\varepsilon_r = 2.2$; $t = 0.8$ mm

——— experimental data

- - - - MoM analysis

a SPA without resonant stubs fed by a 50Ω coaxial probe. The SPA dimensions were $W = 15.5$ mm, $L = 11.5$ mm, $l = 0.5$ mm, $w = d = 1$ mm, $W_p = 5.5$ mm. Two resonances were obtained at $f_{100} = 5.515$ GHz and $f_{300} = 10.446$ GHz (FR = 1.89). The experimental curve (continuous line) compares well with the results obtained by the MoM analysis (dashed line). This and other results [12, 14] provide a validation of the MoM analysis adopted, also used for testing the empirical formulas presented in Section 3. A fairly good simultaneous matching was obtained by using the procedure indicated in Section 5, namely $|S_{11}| = -17$ dB at f_{100} and $|S_{11}| = -14$ dB at f_{300}. The central resonance of lower amplitude that appears in the above Figure is associated with the TM_{200} mode that is excited in the structure owing to the asymmetrical feed.

The narrow bandwidth at the two resonances is due to the small substrate thickness. It is worth noting that the bandwidth of the upper resonance ($\sim 1.2\%$ for VSWR < 2) is wider than that of the lower resonance ($\sim 0.8\%$ for VSWR < 2). This is due to the fact that the substrate is thicker in terms of a wavelength at the upper resonance. In general, the experimental results and the fullwave analysis have shown a bandwidth for the two frequencies that is comparable with that of a rectangular patch, provided that the slots have a width comparable with the thickness of the substrate. Although the bandwidth may be improved by using multilayer configurations, it is worth noting that in many practical applications the use of two separated frequencies allows to relax the bandwidth requirements for each frequency.

Experimental results on a rectangular SPA with resonant tuning stubs are shown in Fig. 9. In this case, the

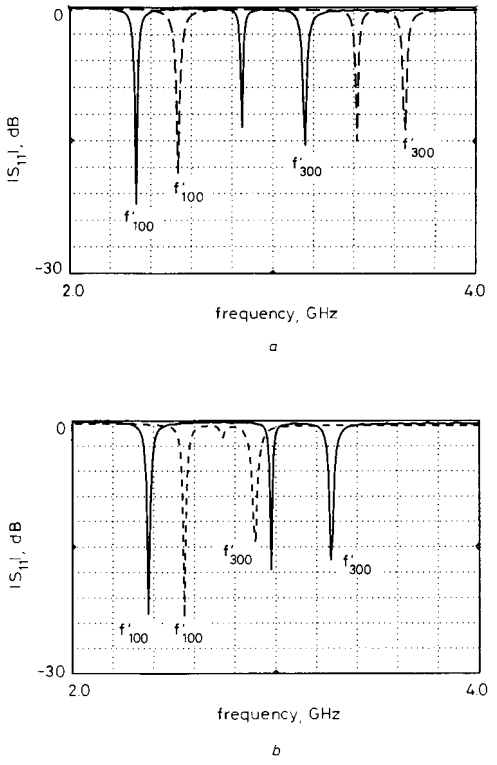

Fig. 9 *Measured amplitude of input reflection coefficient for SPA*

$L = 31$ mm; $W = 42$ mm; $l = w = d = 1$ mm; $\varepsilon_r = \varepsilon'_r = 2.2$; $t = t' = 0.8$ mm with tuning resonators; $L_{ro} = 39.5$ mm; $W_r = 1$ mm

(*a*) - - - - $L_r/L_{ro} = 0.72'$

——— $L_r/L_{ro} = 1.1$

(*b*) ——— $L_v/L_{ro} = 0$

- - - - $L_v/L_{ro} = 0.4$

dimensions of the SPA were $L = 31$ mm, $W = 42$ mm, $l = w = d = 1$ mm. These dimensions correspond to $f_{100} = 2.28$ GHz and $f_{300} = 3.57$ GHz resonances obtained without the tuning stubs. The back substrate was again RT Duroid with $t' = 0.8$ mm and the width of the microstrip tuning stubs was $W_r = 1$ mm, that corresponds to a 83.2 Ω characteristic impedance. A 50 Ω microstrip feed line was connected to the feed point, placed at 15 mm from an edge. The reference length $L_{ro} = 39.5$ mm of the stubs was chosen according to that suggested in eqn. 11. The two curves in Fig. 9*a* show the input reflection coefficient for a stub length L_r greater than and lower than L_{ro}, respectively. The via was initially placed at the end of the stub ($L_v = 0$). For $L_r/L_{ro} = 0.72$ (dashed line) the resonances were found at $f'_{100} = 2.54$ GHz and $f'_{300} = 3.66$ GHz. A relevant shift of the frequencies was observed for $L_r/L_{ro} = 1.1$ (continuous line), i.e. $f'_{100} = 2.34$ GHz and $f'_{300} = 3.17$ GHz. This shows the capability to shift the frequencies position by

changing the stub length. On the other hand, one can change the frequency ratio by varying the via position. Fig. 9*b* shows measurements that are obtained by fixing

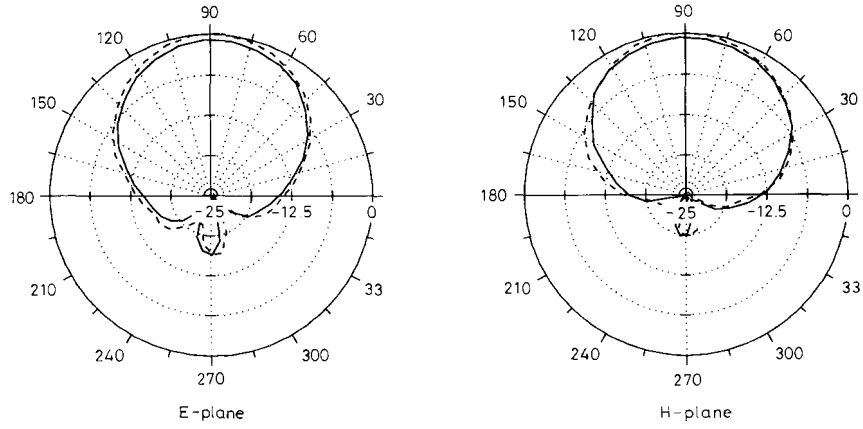

Fig. 10 *Measured radiation patterns for SPA f_{100} = 5.51 GHz; W = 15.5 mm; L = 11.5 mm; l = 0.5 mm; w = 1 mm; d = 1 mm; W_p = 5.5 mm; ε_r = 2.2; t = 0.8 mm and for a standard patch with same resonant frequency; W = 17.75 mm; L = 12.5 mm; W_p = 7.25 mm; ε_r = 2.2; t = 0.8 mm*
—— lotted patch - - - - standard patch

$L_r = L_{ro}$ for two different positions of the vias, namely $L_v = 0$ (continuous line) and $L_v = 0.4 \times L_{ro}$ (dashed line). In this case the frequency ratio changes from $r' = 1.37$ to 1.14.

Finally, the radiation patterns of the SPA in Fig. 8 were measured and compared with those of a patch without slots operating at the same lower frequency (5.51 GHz). To this end, a rectangular patch was realised on the same substrate with dimensions $W = 17.75$ mm, $L = 12.5$ mm, $W_p = 7.25$ mm. The upper frequency (10.44 GHz) of the SPA was designed to satisfy the measurements constraints. Fig. 10 compares the radiation patterns of the two antennas in the *E*-plane (eqn. 14*a*) and in the *H*-plane (eqn. 14*b*). A gain of 6.5 and 7.3 dB was found for the SPA and for the patch without slots, respectively. The introduction of the slots does not affect the radiation pattern of the first mode and produces minor gain losses. The radiation pattern of the SPA in the two principal planes are presented in Figs 11*a* and 11*b*. The dashed and continuous lines correspond to the lower and the upper frequency, respectively; a gain of 6.8 dB was found for the upper frequency. The *E*-plane radiation pattern at the upper frequency is broader than that for the lower frequency. This is probably due to the high frequency ratio that requires slots with dimensions at the upper bound of eqn. 1*a*.

7 Conclusions

A new dual-frequency antenna has been studied that consists of a single layer patch with two narrow slots close to the radiating edges. The lower operating frequency is almost the same as that of a rectangular patch without slots; the upper frequency is well controlled by changing the slots length. The two slots should not be too short or too displaced from the edges to avoid the deformation of the pattern associated with the upper frequency. These restrictions impose a limitation to the FR that has to be lower than 2 and greater than 1.6.

To obtain a more extended range, two tuning microstrip stubs are introduced on a back substrate. Moreover,

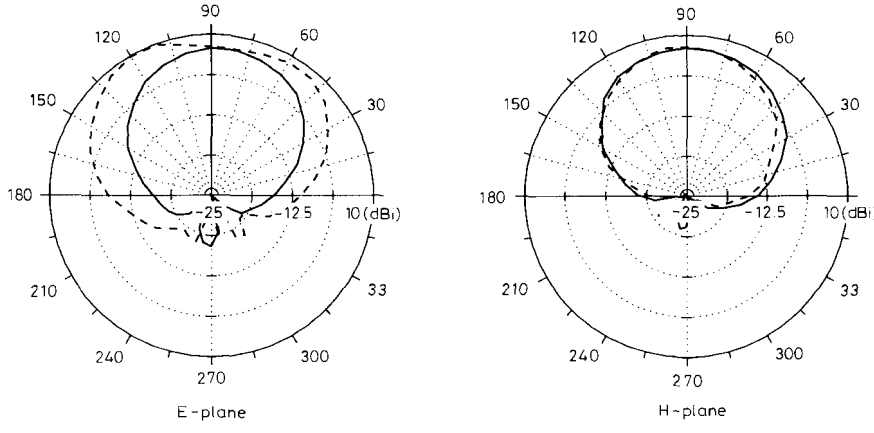

Fig. 11 *Measured gain patterns for SPA*
W = 15.5 mm; *L* = 11.5 mm; *l* = 0.5 mm; *w* = 1 mm; *d* = 1 mm; W_p = 5.5 mm, ε_r = 2.2; *t* = 0.8 mm
—— TM_{100} mode f_{100} = 5.515 GHz - - - TM_{300} mode f_{300} = 10.44 GHz

these allow a simple and accurate design of the two frequencies by means of a CAD software for microwave networks. Finally, a dual-matching capability of the antenna by a single feed point has been demonstrated, both by theoretical and experimental investigation.

Our present efforts are devoted to adapt the structure for dual polarisation by using four slots on a square patch.

8 References

1 LONG, S.A., and WALTON, M.D.: 'A dual-frequency stacked circular-disc antenna', *IEEE Trans.* 1979, **AP-27,** (3), pp. 1281–1285

2 DAHELE, J.S., LEE, K.F., and WONG, D.P.: 'Dual frequency stacked annular-ring microstrip antenna', *IEEE Trans.*, 1987, **AP-35,** (11), pp. 1281–1285

3 WANG, J., FRALICH, R., WU, C., and LITVA, J.: 'Multifunctional aperture coupled stack antenna', *Electron. Lett.*, 1990, **26,** (25), pp. 2067–2068

4 MIRSCHEKAR-SYANKAL, D., and HASSANI, H.R.: 'Characteristics of stacked rectangular and triangular patch antennas for dual band application'. IEE 8th ICAP, Edinburgh, March 1993

5 CROQ, F., and POZAR, D.: 'Multifrequency operation of microstrip antennas using aperture coupled parallel resonators', *IEEE Trans.*, 1992, **AP-40,** (11), pp. 1367–1374

6 RICHARDS, W.F., DAVIDSON, S.E., and LONG, S.A.: 'Dual-band reactively loaded microstrip antenna', *IEEE Trans.*, 1985, **AP-33,** (5), pp. 556–560

7 DAVIDSON, S.E., LONG, S.A., and RICHARDS, W.F.: 'Dual-band microstrip antenna with monolithic reactive loading', *Electron. Lett.*, 1985, **21,** (21), pp. 936–937

8 WATERHOUSE, R.B., and SHULEY, N.V.: 'Dual frequency microstrip rectangular patches', *Electron. Lett.*, 1992, **28,** (7), pp. 606–607

9 ZHONG, S.S., and LO, Y.T.: 'Single element rectangular microstrip antenna for dual-frequency operation', *Electron. Lett.*, 1983, **19,** (8), pp. 298–300

10 SCHAUBERT, D.H., FERRAR, F.G., SINDORIS, A., and HAYES, S.T.: 'Microstrip antennas with frequency agility and polarization diversity', *IEEE Trans.*, 1981, **AP-29,** (1), pp. 118–123

11 WANG, B.F., and LO, Y.T.: 'Microstrip antenna for dual-frequency operation', *IEEE Trans.*, 1984, **AP-32,** (9), pp. 938-943

12 MACI, S., AVITABILE, G., and BIFFI GENTILI, G.: 'Single-layer dual-frequency patch antenna', *Electron. Lett.*, 1993, **29,** (16)

13 YAZIDI, M.L., HIMDI, M., and DANIEL, J.P.: 'Aperture coupled microstrip antenna for dual frequency operation', *Electron. Lett.*, 1993, **29,** (17)

14 MACI, S., AVITABILE, G., BONIFACIO, F., and BORSELLI, L.: 'A multi-resonant slotted patch'. Proceedings of the 23rd European Microwave Conference, Madrid, September 1993

15 RAUTIO, J.C., and HARRINGTON, R.F.: 'An electromagnetic time-harmonic analysis of shielded microstrip circuits', *IEEE Trans.*, 1987, **MTT-35,** (8), pp. 726–730

16 HAMMERSTAD, E.O.: 'Equations for microstrip circuit design', Proceedings of the 5th European Microwave Conference, Hamburg, September 1975, pp. 268–272

17 DERNERYD, A.G.: 'Linearly polarized microstrip antennas', *IEEE Trans.*, 1976, **AP-24,** (11), pp. 846–851

18 DERNERYD, A.G.: 'A theoretical investigation of the rectangular microstrip antenna element', *IEEE Trans.*, 1978, **AP-26,** (7), pp. 532–535

19 DEARNLEY, R.W., and BAREL, A.R.F.: 'A broad-band transmission line model for a rectangular microstrip antenna', *IEEE Trans.*, 1989, **AP-37,** (1), pp. 6–15